Gadolinium-Doped Persistent Nanophosphors as Versatile Tool for Multimodal In Vivo Imaging

Thomas Maldiney, Bich-Thuy Doan, Damien Alloyeau, Michel Bessodes, Daniel Scherman, and Cyrille Richard**

Recent breakthroughs in the rational development of multifunctional nanocarriers have highlightened the advantage of combining the complementary forces of several imaging modalities into one single nanotool fully dedicated to the biomedical field and diagnosis applications. A novel multimodal optical-magnetic resonance imaging nanoprobe is introduced. Designed on the basis of a spinel zinc gallate structure doped with trivalent chromium and gadolinium, this nanocrystal bears the ability to serve as both a highly sensitive persistent luminescence nanoprobe for optical imaging, and a negative contrast agent for highly resolved magnetic resonance imaging (MRI). Additional proof is given that surface coverage can be modified in order to obtain stealth nanoparticles highly suitable for real-time in vivo application in mice, showing delayed reticulo-endothelial uptake and longer circulation time after systemic injection.

1. Introduction

Advances in the intelligent design of highly sophisticated nanocarriers have led to the development of several reliable platforms intended for diagnosis applications.[1] Taking advantage of the large available space within a single nanoparticle, as compared to other systems in the molecular scale, many research groups have pursued the idea that the same rationally engineered cargo could simultaneously carry multiple functions at a time. Thereby, many novel nanotechnologies were lately introduced to serve as multifunctional systems dedicated to either multimodal imaging[2,3] or hybrid imaging/therapeutic theranostic applications.[4,5] In particular, the scientific interest is focusing on the development of multimodal imaging probes associating one high sensitivity modality, such as fluorescence or positron emission tomography (PET) imaging, with one high spatial resolution modality, typically magnetic resonance imaging (MRI).[6]

Recently, our group has introduced the use of persistent luminescence nanoparticles as photonic probes for optical imaging in vivo.[7] These nanomaterials can be excited under a UV lamp before the injection to small animals, and emit a near-infrared persistent luminescence through living tissues, which allows real-time detection with absolute sensitivity as well as complete avoidance of the autofluorescence. We have shown that proper surface functionalization of these nanoparticles could not only be used to favor in vivo long-lasting blood circulation,[8] but also to specifically target cancer cells in vitro.[9,10] In addition, the recent elucidation of the fundamental mechanism driving persistent luminescence phenomenon in diopside host led to an optimization of the crystal co-doping conditions, and unveiled a novel composition, displaying better optical characteristics for in vivo applications.[11,12] Nonetheless, despite these improved characteristics of persistent luminescence materials,[13] the signal could not be followed more than 2 hours in living animals, which impeded long-term biomedical applications such as tumor-targeting. We have recently overcome this limitation by introducing a new generation of non-toxic persistent luminescence nanomaterials, based on trivalent chromium-doped zinc gallate with formula $ZnGa_{1.995}Cr_{0.005}O_4$, which can be excited through living tissues by using low energy photons, in the red region of the visible spectrum.[14,15] This promising nanotechnology is potentially of wide applications to biologists and pharmacologists involved in cancer diagnosis, vascular biology, as well as cell therapy research.

In the present study, we report the synthesis and functionalization of a novel multimodal imaging probe, based on gadolinium-doped persistent nanophosphors, and intended for in vivo diagnosis applications in small animals. This nanocrystal bears the ability to be simultaneously used as optical probe, with the main advantage to allow real-time detection and absolute sensitivity associated with persistent luminescence properties, as well as negative contrast agent for MRI, that brings high spatial resolution along with non invasive anatomical precision.

Dr. T. Maldiney, Dr. B.-T. Doan, Dr. Michel Bessodes, Prof. D. Scherman, Dr. C. Richard
Unité de Technologies Chimiques et Biologiques pour la Santé (UTCBS), CNRS UMR 8258, INSERM U 1022.
Paris F-75270 cedex, France
E-mail: bich-thuy-doan@chimie-paristech.fr; cyrille.richard@parisdescartes.fr

Dr. T. Maldiney, Dr. B.-T. Doan, Dr. Michel Bessodes, Prof. D. Scherman, Dr. C. Richard
Université Paris Descartes
Sorbonne Paris Cité Faculté des Sciences Pharmaceutiques et Biologiques
Paris F-75270 cedex, France

Dr. T. Maldiney, Dr. B.-T. Doan, Dr. Michel Bessodes, Prof. D. Scherman, Dr. C. Richard
Chimie-ParisTech
Paris F-75231 cedex, France

Dr. D. Alloyeau
Laboratoire Matériaux et Phénomènes Quantiques
Université Paris Diderot
Paris F-75205 cedex, France

DOI: 10.1002/adfm.201401612

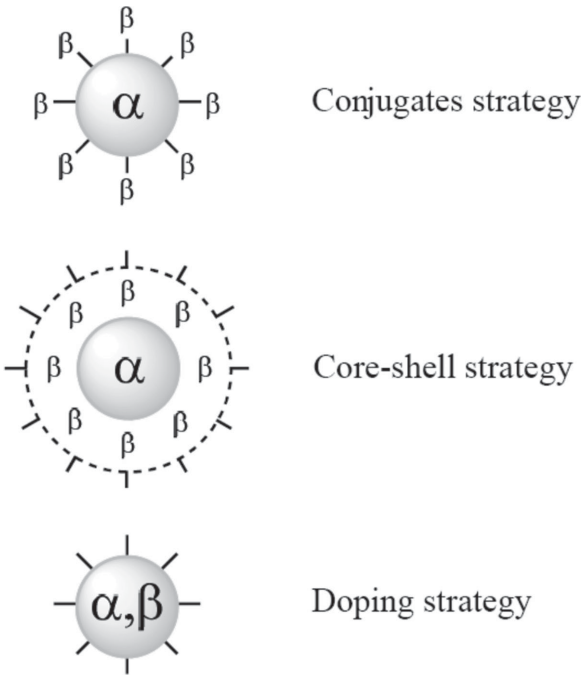

Scheme 1. Schematic representation of the three major strategies employed to conceive a multimodal imaging nanoprobe.

2. Results and Discussion

Three major strategies can lead to the development of an efficient multimodal imaging nanoprobe (**Scheme 1**). The first approach relies on a surface chemical modification of the nanoparticle to add the extra modality as molecular moiety.[16] However, such surface grafting comes necessarily with a significant loss of available functional groups intended for a future functionalization with biological ligands and could hamper targeting perspectives. To circumvent this later limitation and retrieve surface accessibility, a second method can be preferred that consists in the formation of a core-shell structure, with a first modality confined within the core of the nanoparticle, while the other is distributed in the shell.[17] Such strategy, though interesting regarding the accessibility it frees on the surface of the carrier, comes with an inevitable increase in hydrodynamic diameter, depending on the overall shell thickness, that may jeopardize applications in vivo by shortening plasma half-life of the probe. Finally, the doping approach, more challenging given the few reports of success,[18] combines the advantages of the two modalities without any increase in hydrodynamic diameter or decrease in surface accessibility.

2.1. Synthesis of Gd-Doped Persistent Nanophosphors and Physico-Chemical Characterizations

We decided to apply the doping approach to our persistent luminescence nanoparticles. Briefly, nanoparticles with formula $ZnGa_{2(0.9975-x)}Cr_{0.005}Gd_{2x}O_4$ (x = 0, 2, or 4%), referred to as ZGO:Cr^{3+},Gd^{3+} (x%), were synthesized by sintering in air after hydrothermal crystallization of chromium/gadolinium-doped zinc gallate under pressure.[19] Results from X-ray diffraction

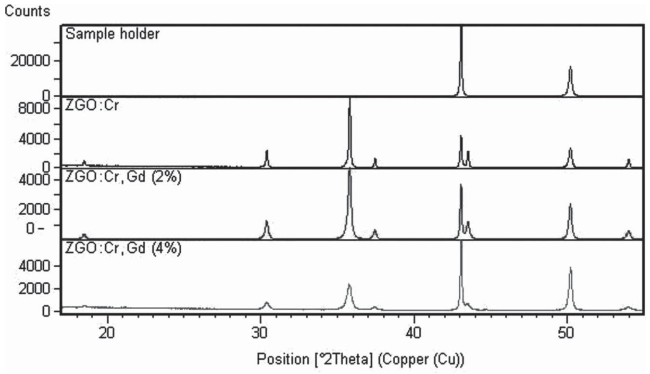

Figure 1. XRD diffractogram of ZGO powders.

(XRD) on bulk powders reveal the formation of pure spinel-type zinc gallate, even after significant gadolinium doping up to 4% (**Figure 1**). We notice from the XRD patterns that the introduction of gadolinium in the structure is responsible for a progressive decline of resolution, with peak intensities gradually decreasing from the compound without gadolinium to the 4%-doped powder. Indeed, given the significant difference between gadolinium (0.938 Å) and gallium (0.62 Å) ionic radii, such change in the diffraction pattern is very certainly associated with a difficult crystallization of the compound probably when trying to force gadolinium in gallium sites. The persistent luminescence decline curves from **Figure 2** corroborate this explanation, as we notice a loss in global signal intensity due to gadolinium doping, no matter which excitation source. Such correlation between optical properties and crystallinity has already been witnessed with several classes of luminescent materials and led to the conclusion that maximum emission intensity was usually achieved when the phosphor exhibited optimal crystallization.[20] Despite this signal loss, Figure 2 shows that gadolinium doping is not leading to a complete quenching of persistent luminescence. Indeed, no matter which excitation source chosen between either red LEDs or UV lamp, persistent luminescence signal remains highly detectable after a two minutes activation of the powders. In addition to these first observations regarding decline kinetics, we also studied the influence of gadolinium content on the optical signature of long-lasting phosphorescence (LLP) emission. Results in Figure S1, Supporting Information,

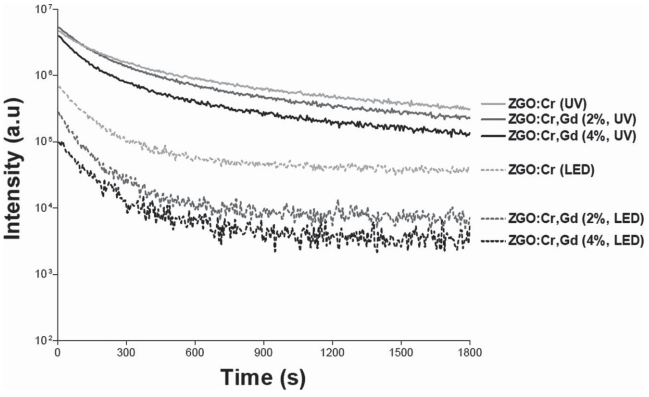

Figure 2. Persistent luminescence decay curves of ZGO nanoparticles.

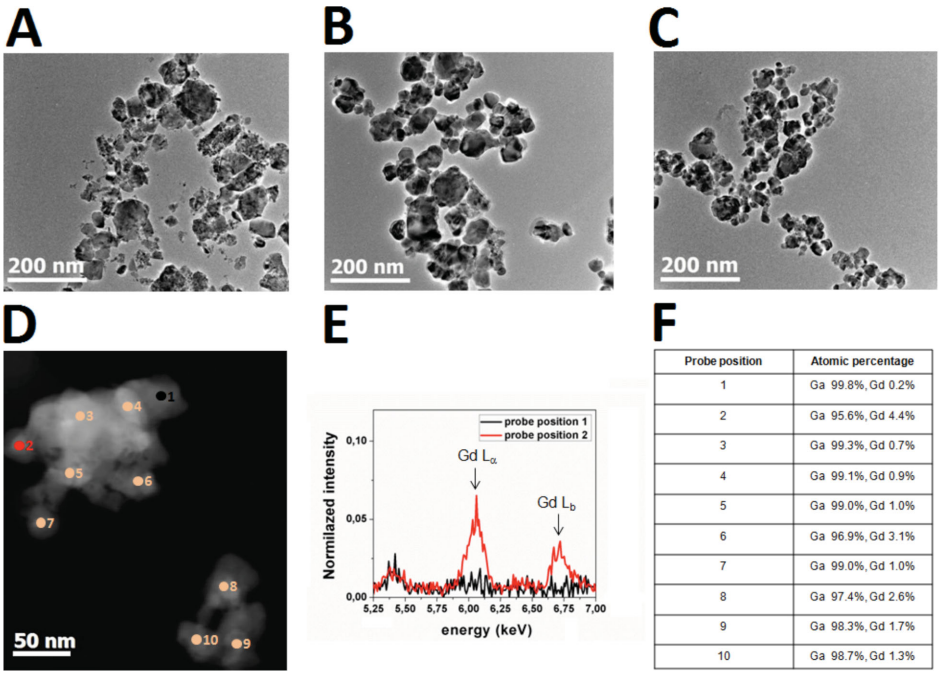

Probe position	Atomic percentage
1	Ga 99.8%, Gd 0.2%
2	Ga 95.6%, Gd 4.4%
3	Ga 99.3%, Gd 0.7%
4	Ga 99.1%, Gd 0.9%
5	Ga 99.0%, Gd 1.0%
6	Ga 96.9%, Gd 3.1%
7	Ga 99.0%, Gd 1.0%
8	Ga 97.4%, Gd 2.6%
9	Ga 98.3%, Gd 1.7%
10	Ga 98.7%, Gd 1.3%

Figure 3. TEM analysis and quantitative STEM – EDX point analyses of Gd-doped $ZnGa_2O_4$ nanoparticles. A–C) Bright field TEM images of the nanoparticles with A) 0%, B) 2% and C) 4% gadolinium. D) STEM image showing the positions of the electron probe during the EDX nano-analyses and the corresponding composition measurements. E) EDX spectra measured at probe position 1 and 2 focused on the energy range of the Gd L_a and L_b peaks. The spectra were normalized with respect to the Ga L_a peak (reference peak intensity above 500 counts). F) quantitative measurements were extracted with the ratio method by using the Cliff-Lorimer factors of the Gd L_a and Ga L_a peaks.

confirm that there is no change in the emission profile of the different compositions. As expected from the relative intensity of LED or UV excited compounds, the less intense was the persistent luminescence signal, the less resolved was the emission spectrum. Precise determination of the gadolinium content of each powder was measured by inductively coupled plasma mass spectrometry (ICP-MS). Results indicate a negligible amount of gadolinium in the compound only doped with chromium, 18.15 mg of Gd^{3+} per gram of 2%-doped compound and 45.37 mg of Gd^{3+} per gram of 4%-doped compound which respectively corresponds to the real percentages of 1.29% and 3.22%. As observed on transmission electron microscopy (TEM) images (**Figure 3**A–C), gadolinium doping does not seem to have any impact on the global size and shape of the nanoparticles. Moreover, energy dispersive X-ray spectroscopy (EDX) measurements were performed over large field of views and revealed a gadolinium percentage of 1% for ZGO:Cr^{3+},Gd^{3+} (2%) and 2% for ZGO:Cr^{3+},Gd^{3+} (4%), which is in the same order of magnitude as the percentages determined from ICP-MS measurements.

In addition, quantitative scanning transmission electron microscopy (STEM) – EDX point analyses were performed to extract quantitative composition measurements on single nano-objects (Figure 3D to F).[21] These results show the inhomogeneous distribution of gadolinium doping in the nanoparticles. The gadolinium composition with respect to the gallium composition ranges from 0.25% (probe position 1) to 4.4% (probe position 2). Unfortunately, the high beam sensitivity of the nanoparticles prevented gadolinium distribution mapping at the nanometer scale using EDX spectrum imaging.

In vivo applications in living animals with such persistent luminescence materials are usually achieved through the extraction of nanoparticles' monodisperse distributions.[8] Such size selection allows removing the aggregates, thus improving chances to get a homogeneous distribution of the probes in vivo. Thereby, we selected the same monodisperse distribution for each compound, with a mean hydrodynamic diameter of 60 nm (Figure S2, Supporting Information). T_1 and T_2-weighted magnetic resonance images presented in **Figure 4**A were recorded at 7T with stable colloidal solutions of ZGO nanoparticles in diluted sodium hydroxide (5 mM). The images reveal a significant effect of gadolinium-doping on both longitudinal and transversal relaxation times. Interestingly, a percentage of gadolinium as low as about 1.3%, reached with ZGO:Cr,Gd (2%), seems to induce a noticeable effect of nanoparticles as positive and negative contrast agent. Quantitative measurements of relaxometry performed at 7T (Figure 4A) confirm a linear dependence of relaxation rates (R_1 and R_2) regarding nanoparticles concentration. In both cases, the more gadolinium enters the zinc gallate structure, the more important the relaxation rates (Figure 4B,C). By contrast, we notice that chromium-doped ZGO nanoparticles, without gadolinium, do not have any influence on the relaxation times of water protons, either T_1 or T_2. Indeed, the magnetic moment of Cr^{3+} is weaker than that of Gd^{3+}, with 4 unpaired electrons for Cr^{3+} compared to 7 for Gd^{3+}. Although trivalent chromium is usually listed among classical paramagnetic species with putative MRI applications,[22] the relative low concentration of dopant used to confer optical signature and final persistent luminescence characteristics to the crystals is not sufficient to provide

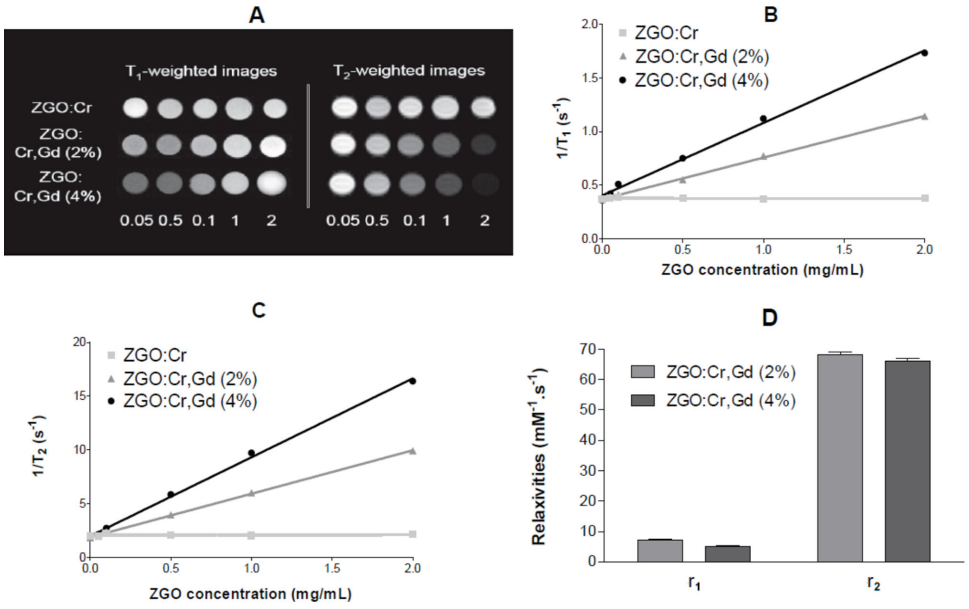

Figure 4. Magnetic properties of ZGO nanoparticles. A) T_1 and T_2-weighted images of ZGO nanoparticles for various concentrations of nanoparticles (T = 25 °C). B) Plots of R_1 values as a function of the nanoparticles concentration expressed in mg ml^{-1}. C) Plots of R_2 values as a function of the nanoparticles concentration expressed in mg ml^{-1}. D) Relaxivities r_1 and r_2 of ZGO nanoparticles suspended in 5 mM NaOH at 7T (T = 25 °C).

substantial magnetic properties to the probe. A final comparison of relaxivities, calculated from relaxation rates curves presented in Figure 4B,C, is given in Figure 4D. The introduction of gadolinium content in chromium-doped persistent luminescence nanoparticles is responsible for a global increase of both longitudinal and transversal relaxivities (around 5 mM^{-1} s^{-1} for r_1 and above 60 mM^{-1} s^{-1} for r_2), while compounds only doped with chromium display almost null r_1 and r_2 (data not shown). In the case of longitudinal and transversal relaxations, increasing gadolinium content does not change the relaxivities of ZGO nanoparticles, and the r_2/r_1 ratio remains close to 11, no matter which gadolinium concentration. Such value of the ratio, combined with the pronounced negative contrast obtained in T_2-weighted images (Figure 4A), strongly suggests a further use of these gadolinium/chromium-doped ZGO nanoparticles as multimodal optical imaging probe and negative T_2-contrast agent for magnetic resonance diagnosis applications in living animals. Noteworthy, gadolinium-based contrast agents, either molecular (Gd-DTPA)[23] or in the form of small nanoparticles[2,24] (2–3 nm Gd_2O_3), usually display rather low r_2/r_1 ratios, i.e., inferior or equal to 1, associated with a global tendency to act as positive T_1-MRI contrast agent. This trend is quite different from the one we observed with gadolinium-doped zinc gallate nanoparticles, which could be the result of size-effects responsible for a significant change in surface/volume phenomenon.[25] Indeed, surface effects being preponderant when decreasing the size of nanoparticles, protons relaxation is mostly driven by the direct interaction between water protons from the biological environment and gadolinium on the surface of the nanoparticle. On the contrary, a significant increase in nanoparticles' diameter leads to the decrease in surface/volume ratio along with a loss of the dominant interaction between protons and surface gadoliniums. In the case of gadolinium-doped ZGO nanoparticles, in which the volume effects are prevailing, the resulting MRI T_2-effect is most likely associated with the strong interaction between the global magnetic moment of nanoparticles, which generates a local magnetic field inhomogeneity, and water protons from the solvent. Following the inner sphere theory of relaxation, individual Gd^{3+} induce paramagnetic relaxation originating from the dipole-dipole interaction between the nuclear spins of the first coordination sphere (^1H of water) and the electron spins of the paramagnetic specie (Gd^{3+}). By contrast, paramagnetic centers confined into a nanosized crystal generate a cooperative effect, commonly observed in inorganic ferrites such as Fe_3O_4, responsible for a strong magnetic moment of the nanoparticle and a predominant transverse relaxation. In relation to the outer sphere relaxation theory, these species are known as superparamagnetic.[26]

2.2. In Vivo Multimodal Imaging

The optical and magnetic properties of the two compositions, ZGO:Cr,Gd (2%) and ZGO:Cr,Gd (4%), were then compared in vivo. First, we investigated the ability of these nanoparticles to be monitored in vivo as optical probe. Nanoparticles from both compositions were suspended in 5% glucose solution, excited under UV light (6W, 254 nm) for 2 minutes, and injected in the tail vein of healthy BALB/c mice. Persistent luminescence images and accumulation kinetics are presented in **Figure 5**. We notice from Figure 5A that ZGO:Cr,Gd (4%) nanoparticles are clearly detectable through living tissues with absolute sensitivity. After a short 5 minutes period, a significant amount of nanoparticles was trapped in liver. The image acquired 45 minutes after the systemic injection confirms an exclusive retention of the nanoparticles within the main reticulo-endothelial system (RES) organs, liver and spleen. Images recorded following

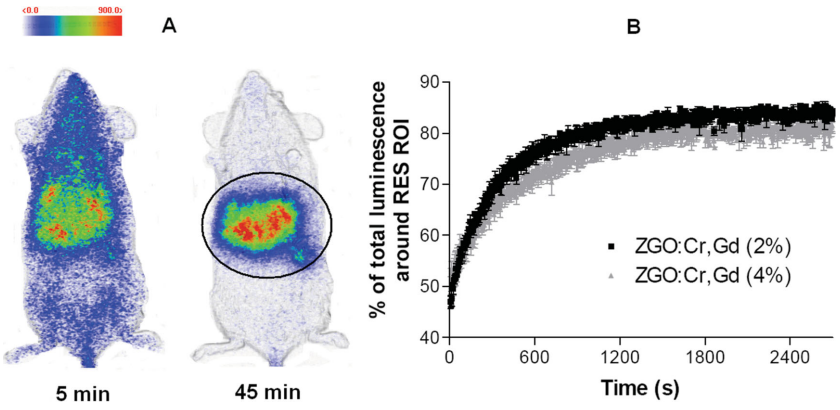

Figure 5. Optical detection of ZGO nanoparticles in vivo. A) Persistent luminescence images 5 and 45 minutes following the injection of UV-excited ZGO:Cr,Gd (4%) nanoparticles (n = 3). Black circle corresponds to a global region of interest (ROI) comprising liver and spleen. B) Accumulation kinetics of gadolinium-doped ZGO nanoparticles within ROI.

the injection of the other composition, ZGO:Cr,Gd (2%), displayed the same biodistribution pattern (data not shown). Such behavior of nanoparticles covered with hydroxyl groups after intravenous injection has already been observed with previous persistent luminescence nanoparticles, based on diopside host.[8] Briefly, this uptake of nanoparticles by RES is very likely the result of a recognition process initiated by the interaction of nanoparticles with opsonins circulating in the blood that finally triggers their capture by phagocytes located within major RES organs, mainly Kupffer cells in liver and splenic macrophages in spleen.

Semi-quantitative analysis of persistent luminescence images allows accurate determination of the amount of nanoparticles confined in a given region of interest (ROI), compared to the whole mouse. After a preliminary ROI delimitation of the main RES organs (Figure 5A), this analysis method was used to monitor global accumulation kinetics of persistent luminescence nanoparticles in liver and spleen (Figure 5B). As expected in view of the similar hydrodynamic diameters and surface characteristics of ZGO:Cr,Gd (2%) and ZGO:Cr,Gd (4%), both compositions display identical accumulation kinetics in RES organs. In particular, a focus on the first 10 minutes of the accumulation curves allows unraveling the mean blood half-life of ZGO nanoparticles, estimated to be about 30 seconds. After 30 minutes, more than 80% of the total luminescence are retrieved in liver and spleen. As the amount of nanoparticles in liver and spleen remains unchanged after 45 minutes, we decided to acquire magnetic resonance images a few minutes later.

T_2*-weighted magnetic resonance images of mice abdominal cross section are presented in **Figure 6**. For each composition and each mouse of the group, a reference image was recorded

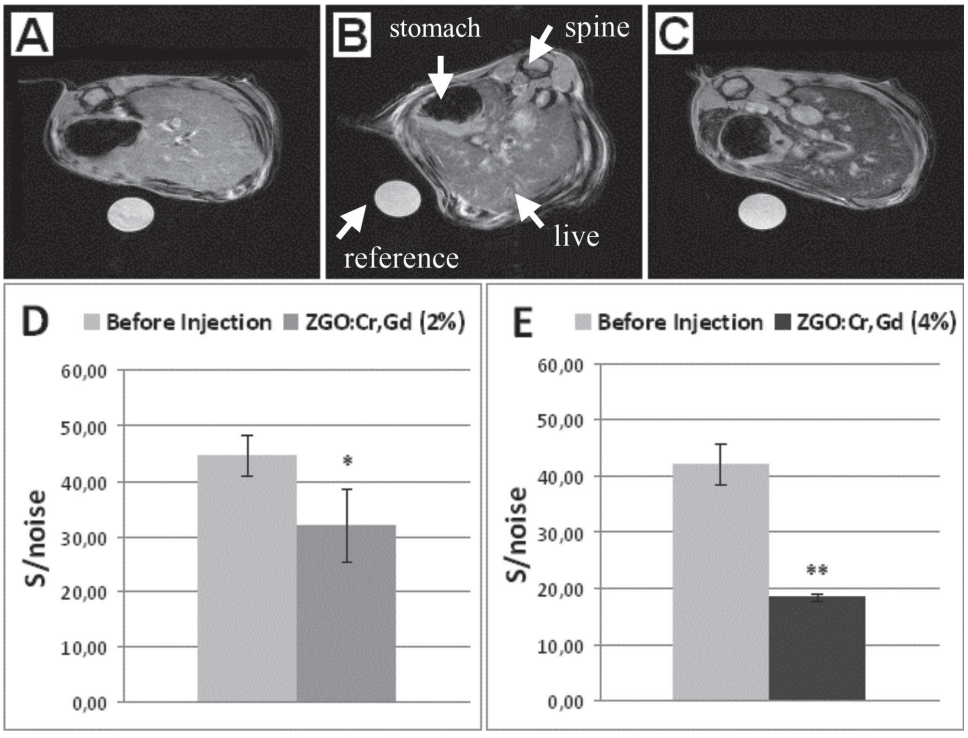

Figure 6. MRI-based detection of ZGO nanoparticles in vivo. T_2* axial MR images of mice liver recorded at 7T (n = 3). A) Reference mouse before the injection of ZGO nanoparticles. B) Reference mouse, 1 hour after the injection of ZGO:Cr,Gd (2%) nanoparticles. C) Reference mouse, 1 hour after the injection of ZGO:Cr,Gd (4%) nanoparticles. D) Comparison of the mean signal/noise from T_2*-weighted images ROI in mouse liver before and after the injection of ZGO:Cr,Gd (2%) nanoparticles. E) Comparison of the mean signal/noise from T_2*-weighted images ROI in mouse liver before and after the injection of ZGO:Cr,Gd (4%) nanoparticles. A reference tube was used for additional signal normalization.

before the intravenous injection of magnetic persistent luminescence nanoparticles. Comparison of Figure 6A, reference image before the injection, with Figure 6B,C, after the injection of ZGO:Cr,Gd (2%) and ZGO:Cr,Gd (4%) nanoparticles, clearly reveals a strong change in contrast within liver. The significant drop in signal to noise ratio, as compared to the reference mouse, evolves from 30% after the injection of ZGO:Cr,Gd (2%) nanoparticles (Figure 6D) to 60% with ZGO:Cr,Gd (4%) nanoparticles (Figure 6E), which represents a doubled value in comparison to the 2%-doped compound. Indeed, in terms of relaxivity expressed per weight of nanoparticles, ZGO:Cr,Gd (4%) nanoparticles are twice more efficient as MRI contrast agent compared to ZGO:Cr,Gd (2%) nanoparticles. Without gadolinium, the ZGO:Cr nanoparticles show no magnetic properties for MRI. Notably, the ZGO:Cr,Gd (4%) nanoparticles are responsible for a strong negative contrast within liver tissues (Figure 6C), with a highly darkened and emphasized surface, as compared to liver vascularization. The magnetic resonance images, obtained from mice abdominal cross section, perfectly correlate results from Figure 5, as well as the persistent luminescence images recorded from in situ activation of the nanoparticles through living tissues, both in vivo and ex vivo, 24 hours after their injection (Figure S3A,B, Supporting Information). This global result constitutes the first report of multimodal imaging nanoparticles, based on red-excitable magnetic persistent luminescence nanoparticles, for optical-MRI detection. These novel nanoprobes not only ensure absolute detection through living tissues by using persistent luminescence, but also serve as negative contrast agent for MRI-based detection with high spatial in vivo resolution, raising thrilling perspectives for bioimaging in living animals. Note that in vivo cellular and systemic toxicity of ZGO-based nanoparticles have already been explored in a previous study that reported neither acute nor long-term toxicity of these optical nanoprobes, assessed by both biomarkers dosage from the liver and histopathological exploration of the main accumulation organs.[14]

Most biological applications of nanoparticles require surface functionalization to provide either good stability in physiological medium, interesting targeting properties for in vitro binding studies, or stealth character to ensure a proper biodistribution in vivo.[27] Focusing on the use of magnetic persistent luminescence nanoparticles for in vivo bioimaging, we finally investigated, as a proof of concept, the ability to confer a stealth character to these nanoprobes in order to favor their biodistribution after systemic injection. Functionalization with polyethylene glycol (PEG) was performed on ZGO:Cr,Gd (4%) nanoparticles, providing the best contrast for MRI in vivo as well as absolute sensitivity for optical detection of persistent luminescence in healthy mice, via a two steps reaction route (**Figure 7**A). Each functionalization step was characterized by zeta potential measurements. Hydroxyl-terminated nanoparticles displayed slightly positive surface charge (25.2 ± 2.38 mV). The condensation of amino-silanes is responsible for a major increase in global surface charge rising up to 38.6 ± 1.84 mV due to the presence of primary amines covering the probes. Finally, PEG grafting allows complete charge masking, with a global zeta potential dropping to the value of 0.867 ± 0.992 mV.

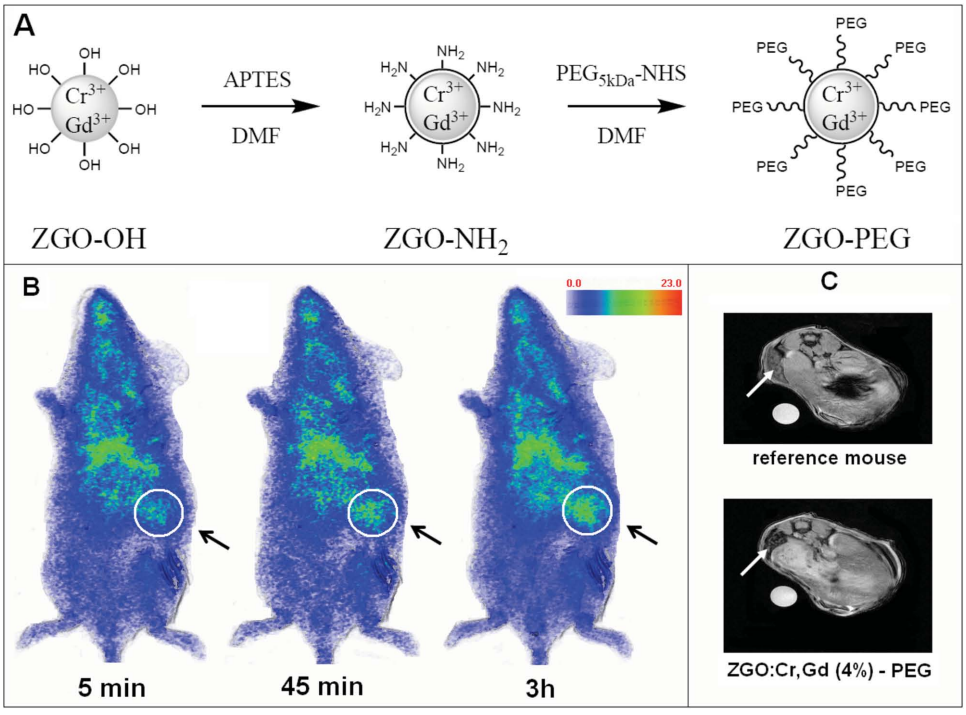

Figure 7. In vivo experiments with ZGO:Cr,Gd (4%)-PEG nanoparticles. A) Schematic representation of ZGO:Cr,Gd (4%) surface functionalization. B) Persistent luminescence images 5, 45 and 180 minutes following the injection of UV-excited ZGO:Cr,Gd (4%)-PEG nanoparticles. Black arrow indicates the region corresponding to spleen. C) Mice liver/spleen T_2*-weighted axial MR images recorded at 7T, 3.5 hours following the injection of ZGO:Cr,Gd (4%)-PEG nanoparticles.

Classical physico-chemical measurements using dynamic light scattering confirm the formation of a thick PEG layer on the surface of the nanoparticles (Figure S4, Supporting Information).

Following the same approach as the one applied for hydroxyl-terminated nanoparticles, we first used the persistent luminescence signal after UV excitation, prior to systemic injection, to monitor short-term biodistribution of the nanoparticles in vivo. Images obtained from the optical detection of the nanoparticles are presented in Figure 7B. Interestingly, a close comparison of the images obtained 5 min, 45 min, and 3 hours after the injection seems to indicate a slow and progressive accumulation of the nanoparticles in spleen (black arrow in the Figure 7B), without noticeable retention within liver. This observation was confirmed by MRI a few minutes later. T_2*-weighted abdominal transversal images of the same mouse (Figure 7C) clearly indicates a significant loss in signal to noise ratio homogeneously located within spleen (white arrow in the Figure 7C), compared to the reference mouse before the injection. However, such visible changes in negative contrast around the liver were not detected by MRI, comforting the results obtained from optical detection performed with persistent luminescence, and the ability of stealth nanoparticles to successfully evade liver defense system and delay their final uptake by Kupffer cells. Such in vivo behavior raises promising perspective for a further use of these stealth nanoparticles to passively target the tumor microenvironment.

3. Conclusion

We have introduced the first multimodal optical-magnetic resonance imaging nanoprobe based on red-excitable magnetic persistent luminescence nanoparticles. This novel generation of gadolinium-doped imaging probes allows not only real-time optical detection through living tissues with absolute sensitivity, but also magnetic resonance imaging with high spatial resolution in vivo. In addition, we have shown that successful surface PEG grafting could be used to greatly increase the circulation time and modulate the biodistribution of these magnetic persistent luminescence nanoparticles after systemic injection to healthy mice, and significantly delay the reticulo-endothelial system uptake in vivo. The development of this new nanotechnology opens thrilling alternatives to a large panel of diagnosis techniques in the field of biomedical research.

Supporting Information

Supporting Information is available from the Wiley Online Library or from the author.

Acknowledgements

We thank Johanne Seguin for her help performing in vivo experiments; Bruno Viana and Laurent Michely for persistent luminescence emission spectra and ICP-MS measurements; René Lai-Kuen and Bruno Saubamea from Technical Platform of the IFR71/IMTCE–Cellular and Molecular Imaging–Faculty of Pharmacy–Paris Descartes University. This work has been supported by the French National Agency (ANR) in the frame of its program in Nanosciences and Nanotechnologies (NATLURIM project no. ANR-08-NANO-025). We are grateful to Region Ile-de-France for convention SESAME E1845, for the support of the JEOL ARM 200F electron microscope installed at the Paris Diderot University.

Received: May 19, 2014
Revised: July 17, 2014
Published online: November 20, 2014

[1] R. Weissleder, M. J. Pittet, *Nature* **2008**, *452*, 580.
[2] J. L. Bridot, A. C. Faure, S. Laurent, C. Rivière, C. Billotey, B. Hiba, M. Janier, V. Josserand, J. L. Coll, L. V. Elst, R. Muller, S. Roux, P. Perriat, O. Tillement, *J. Am. Chem. Soc.* **2007**, *129*, 5076.
[3] X. Lin, J. Xie, G. Niu, F. Zhang, H. Gao, M. Yang, Q. Quan, M. A. Aronova, G. Zhang, S. Lee, R. Leapman, X. Chen, *Nano Lett.* **2011**, *11*, 814.
[4] N. Sanvicens, M. P. Marco, *Trends Biotechnol.* **2008**, *26*, 425.
[5] E. Tasciotti, X. Liu, R. Bhavane, K. Plant, A. D. Leonard, B. K. Price, M. M. Cheng, P. Decuzzi, J. M. Tour, F. Robertson, M. Ferrari, *Nat. Nanotechnol.* **2008**, *3*, 151.
[6] A. Louie, *Chem. Rev.* **2010**, *110*, 3146.
[7] Q. le Masne de Chermont, C. Chanéac, J. Seguin, F. Pellé, S. Maîtrejean, J. P. Jolivet, D. Gourier, M. Bessodes, D. Scherman, *Proc. Natl. Acad. Sci. USA* **2007**, *104*, 9266.
[8] T. Maldiney, C. Richard, J. Seguin, N. Wattier, M. Bessodes, D. Scherman, *ACS Nano.* **2011**, *5*, 854.
[9] T. Maldiney, G. Byk, N. Wattier, J. Seguin, R. Khandadash, M. Bessodes, C. Richard, D. Scherman, *Int. J. Pharm.* **2012**, *423*, 102.
[10] T. Maldiney, M. U. Kaikkonen, J. Seguin, Q. le Masne de Chermont, M. Bessodes, K. J. Airenne, S. Ylä-Herttuala, D. Scherman, C. Richard, *Bioconjug. Chem.* **2012**, *23*, 472.
[11] T. Maldiney, A. Lecointre, B. Viana, A. Bessière, M. Bessodes, D. Gourier, C. Richard, D. Scherman, *J. Am. Chem. Soc.* **2011**, *133*, 11810.
[12] T. Maldiney, A. Lecointre, B. Viana, A. Bessière, D. Gourier, M. Bessodes, C. Richard, D. Scherman, *Proc. SPIE* **2012**, *8263*, 826318f.
[13] T. Maldiney, G. Sraiki, B. Viana, D. Gourier, C. Richard, D. Scherman, M. Bessodes, K. Van den Eeckhout, D. Poelman, P. F. Smet, *Opt. Mater. Express.* **2012**, *2*, 261.
[14] T. Maldiney, A. Bessière, J. Seguin, E. Teston, S. K. Sharma, B. Viana, A. J. Bos, P. Dorenbos, M. Bessodes, D. Gourier, D. Scherman, C. Richard, *Nat. Mater.* **2014**, *13*, 418.
[15] A. Bessière, S. K. Sharma, N. Basavaraju, K. R. Priolkar, L. Binet, B. Viana, A. J. Bos, T. Maldiney, C. Richard, D. Scherman, D. Gourier, *Chem. Mater.* **2014**, *26*, 1365.
[16] T. Jin, Y. Yoshioka, F. Fujii, Y. Komai, J. Seki, A. Seiyama, *Chem. Commun.* **2008**, 5764.
[17] J. Kim, H. S. Kim, N. Lee, T. Kim, H. Kim, T. Yu, I. C. Song, W. K. Moon, T. Hyeon, *Angew. Chem. Int. Ed. Engl.* **2008**, *47*, 8438.
[18] X. Zhang, M. Brynda, R. D. Britt, E. C. Carroll, D. S. Larsen, A. Y. Louie, S. M. Kauzlarich, *J. Am. Chem. Soc.* **2007**, *129*, 10668.
[19] X. Zhang, J. Huang, K. Ding, Y. Hou, X. Wang, X. Fu, *Environ. Sci. Technol.* **2009**, *43*, 5947.
[20] A. Lakshmanan, *Sintering of Ceramics – New Emerging Techniques*, InTech, **2002**.

[21] D. Alloyeau, G. Prévot, Y. Le Bouar, T. Oikawa, C. Langlois, A. Loiseau, C. Ricolleau, *Phys. Rev. Lett.* **2010**, *105*, 255901.
[22] G. E. Jackson, M. J. Byrne, G. Blekkenhorst, A. J. Hendry, *Int. J. Rad. Appl. Instrum. B.* **1991**, *18*, 855.
[23] P. Caravan, *Chem. Soc. Rev.* **2006**, *35*, 512.
[24] G. K. Das, B. C. Heng, S. C. Ng, T. White, J. S. Loo, L. D'Silva, P. Padmanabhan, K. K. Bhakoo, S. T. Selvan, T. T. Tan, *Langmuir* **2010**, *26*, 8959.
[25] B. H. Kim, N. Lee, H. Kim, K. An, Y. I. Park, Y. Choi, K. Shin, Y. Lee, S. G. Kwon, H. B. Na, J. G. Park, T. Y. Ahn, Y. W. Kim, W. K. Moon, S. H. Choi, T. Hyeon, *J. Am. Chem. Soc.* **2011**, *133*, 12624.
[26] A. S. Merbach, L. Helm, E. Toth, *The Chemistry of Contrast Agents in Medical Magnetic Resonance Imaging*, John Wiley and Sons, **2013**.
[27] A. A. Guay-Bégin, P. Chevallier, L. Faucher, S. Turgeon, M. A. Fortin, *Langmuir* **2012**, *28*, 774.